Chemistry–A European Journal
Research Article
doi.org/10.1002/chem.202303549
Chemistry Europe
European Chemical Societies Publishing
www.chemeurj.org

3,4-Dimethylenecyclobutene: A Building Block for Design of Macrocycles with Excited State Aromatic Low-Lying High-Spin States

Preethanuj Preethalayam,[a] Juan Carlos Roldao,[a, b, c] Frédéric Castet,[c] David Casanova,*[b, d] Slavko Radenković,*[e] and Henrik Ottosson*[a]

3,4-Dimethylenecyclobutene (**DMCB**) is an unusual isomer of benzene. Motivated by recent synthetic progress to substituted derivatives of this scaffold, we carried out a theoretical and computational analysis with a particular focus on the extent of (anti)aromatic character in the lowest excited states of different multiplicities. We found that the parent **DMCB** is non-aromatic in its singlet ground state (S_0), lowest triplet state (T_1), and lowest singlet excited state (S_1), while it is aromatic in its lowest quintet state (Q_1) as this state is represented by a triplet multiplicity cyclobutadiene (**CBD**) ring and two uncoupled same-spin methylene radicals. Interestingly, the Q_1 state, despite having four unpaired electrons, is placed merely 4.8 eV above S_0, and there is a corresponding singlet tetraradical 0.16 eV above. The **DMCB** is potentially a highly useful structural motif for the design of larger molecular entities with interesting optoelectronic properties. Here, we designed macrocycles composed of fused **DMCB** units, and according to our computations, two of these have low-lying nonet states (*i.e.*, octaradical states) at energies merely 2.40 and 0.37 eV above their S_0 states as a result of local Hückel- and Baird-aromatic character of individual 6π- and 4π-electron monocycles.

Introduction

3,4-Dimethylenecyclobutene (**DMCB**, Figure 1) is a benzene isomer which has received less attention in the literature than isomers such as fulvene, Dewar-benzene, and prismane. This fully π-conjugated hydrocarbon has two exocyclic CC double bonds that expand out of a cyclobutene ring,[1–14] and efficient synthesis of a variety of **DMCB** derivatives via a palladium-catalyzed coupling reaction was recently reported by Huang *et al.*[15] Thus, synthetic progress has opened doors to a largely unexplored molecular scaffold with, as we reveal herein, unique excited state features.

From early on, the parent **DMCB** has been purported as antiaromatic in its singlet ground state (S_0),[11] although this classification does not hold true to a qualitative analysis in the framework of Hückel's rule because the four-membered ring (4-MR) is not a cycle of alternating CC single and double bonds typical of an antiaromatic [4*n*]annulene. Even though **DMCB** has four sp^2 hybridized C atoms in the 4-MR cyclic structure, two of these atoms are part of exocyclic C=C bonds. Interestingly though, **DMCB** is not cross-conjugated but omni-conjugated, meaning that all C atoms are linearly conjugated to each other.[16] Indeed, an antiaromatic character can only result if structures that are either diradical or zwitterionic at the two exocyclic C atoms make substantial contributions to the electronic ground state (structures **S_0-VIII**–**S_0-IX**, Figure 1). One may, however, ask if these structures are representative of the S_0 state of **DMCB**. They have a lower number of π-bonds than **S_0-I**, and structure **S_0-IX** also implies charge separation. These are features which, in addition to the alleged antiaromatic character, would lead to a low stability of **DMCB** in S_0.

Yet, small antiaromatic compounds such as cyclobutadiene (**CBD**) and pentalene only exist at cryogenic temperatures (*e.g.*, **CBD** dimerizes at 35 K),[17,18] unless stabilized kinetically by bulky substituents or/and benzannelation.[19–26] In contrast, **DMCB** kept under nitrogen can be stored at ambient temperatures for long periods and it is stable up until 375 °C.[5,9] This high persistence speaks against it being antiaromatic, and it should likely be labelled as nonaromatic in S_0, in contrast to how it has been labelled earlier.[11,15,27–31] Following Hückel's rule, **DMCB** may instead have some antiaromatic character in the lowest triplet state (T_1), although this requires that the triplet diradical

[a] *P. Preethalayam, J. C. Roldao, H. Ottosson*
Department of Chemistry – Ångström Laboratory, Uppsala University, Uppsala, Sweden
E-mail: henrik.ottosson@kemi.uu.se
[b] *J. C. Roldao, D. Casanova*
Donostia International Physics Center (DIPC), 20018 Donostia, Euskadi, Spain
[c] *J. C. Roldao, F. Castet*
University of Bordeaux, CNRS, Bordeaux INP, ISM, UMR 5255, F-33405 Cedex Talence, France
[d] *D. Casanova*
IKERBASQUE – Basque Foundation for Science, 48009 Bilbao, Euskadi, Spain
E-mail: david.casanova@dipc.org
[e] *S. Radenković*
University of Kragujevac, Faculty of Science, P. O. Box 60, 34000 Kragujevac, Serbia
E-mail: slavkoradenkovic@kg.ac.rs
Supporting information for this article is available on the WWW under https://doi.org/10.1002/chem.202303549

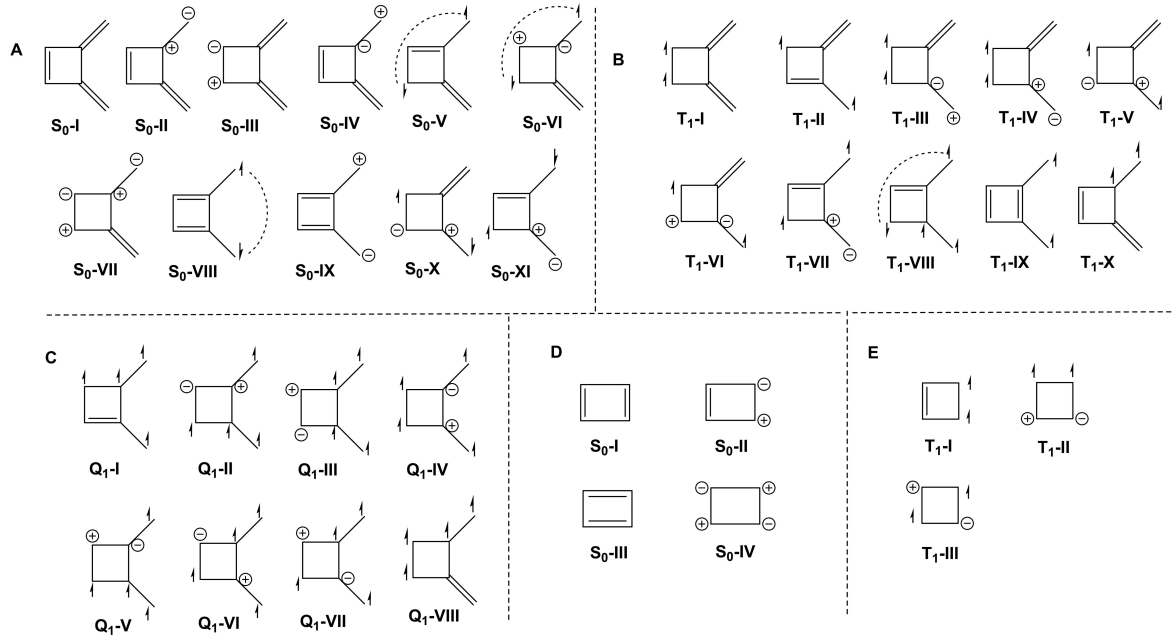

Figure 1. Various valence bond structures of **DMCB** and **CBD** in their singlet ground state (S_0), the lowest triplet (T_1), and quintet (Q_1 for **DMCB**) states, showing their potential non-aromatic, Hückel antiaromatic, and Baird aromatic characters. Only non-equivalent structures are represented.

character localizes at the two exocyclic C atoms (structure **T_1-IX**). If so, one may ask in which state **DMCB** exhibits Baird-aromatic character. From simple reasoning it is apparent that the Baird-aromatic character, which requires a 4π-electron cycle with three π_α electrons and one π_β, can be achieved for states with quintet multiplicity (structure **Q_1-I**) as well as open-shell tetraradical singlet states. Of these, the quintet state would have two π_α electrons at the exocyclic C atoms and a CBD ring with local triplet multiplicity (three π_α and one π_β electron), which is Baird-aromatic. The open-shell singlet state, on the other hand, could be Baird-aromatic in the CBD ring if the two unpaired electrons at the exocyclic C atoms have spins so that the total multiplicity becomes singlet.[32]

Our ongoing interest in excited state (anti)aromaticity,[33–36] and in the chemistry of cross-conjugated species such as fulvenes,[37–40] prompted us to investigate the behavior of **DMCB** in its S_0 state and the lowest excited singlet (S_1), triplet (T_1) and quintet (Q_1) states. The first goal is to reveal the details of the parent **DMCB** (anti)aromaticity in the different electronic states. Building on our findings of the parent **DMCB**, we then analyze a series of **DMCB**-based macrocyclic compounds with low-lying high-spin states (nonet states) with monocycles that have, respectively, local closed-shell singlet Hückel-aromatic character and open-shell triplet Baird-aromatic character. Present **DMCB** derivatives are stable at ambient temperatures/conditions when aryl substituted, yet, the 4-MRs in the macrocyclic compounds investigated may require additional sterically congestive groups. As it is known that this kinetic stabilization yields **CBD**s which are stable at ambient temperatures,[41–44] we postulate that the macrocycles with low-lying nonet states can be realistic.

Results and Discussion

In the first section we analyze the fundamental properties of the parent **DMCB** in its ground and low-lying excited states with different spin multiplicities. This analysis provides a basis for the subsequent computational design of macrocycles with low-lying excited states of very high multiplicity (nonet states). The computations were carried out with both (TD)DFT using the B3LYP and ωB97X-D[45–47] as well as wavefunction methods (valence bond theory and coupled cluster methods).[48–56] For the (anti)aromaticity analysis we utilized indices that reveal the energetic, electronic, geometric, and magnetic aspects of aromaticity.[57–72] The computations were done with the Gaussian16, Q-Chem, and XMVB 3.0 program packages.[73–76] For further computational details see the Supporting Information.

Several questions emerge when considering the (anti)aromatic character of **DMCB**, especially in comparison to **CBD**. To what extent is **DMCB** antiaromatic in S_0? To what extent is it Baird-aromatic in the excited states, and can this be rationalized qualitatively? Do various aromaticity indices that represent the different aspects of aromaticity provide consistent answers on the extent of (anti)aromaticity? If not, can the differences be rationalized?

Nature of the DMCB ground state: The ground state geometry of **DMCB** is fully planar like **CBD**, but with a lower C_{2v} symmetry imposed by the dimethylene substitution (Figure 2A and Figure S3), as revealed by the non-vanishing dipole moment of 0.68 D (Table 1). Furthermore, **DMCB** has a rather different bond length pattern, with one short CC bond (the C1–C2 bond, Figure 2A and Figure S7), closer to a linear conjugation of a 1,3,5-hexatriene unit than the 4-MR cyclic conjugation of **CBD**. Although the value of the geometric

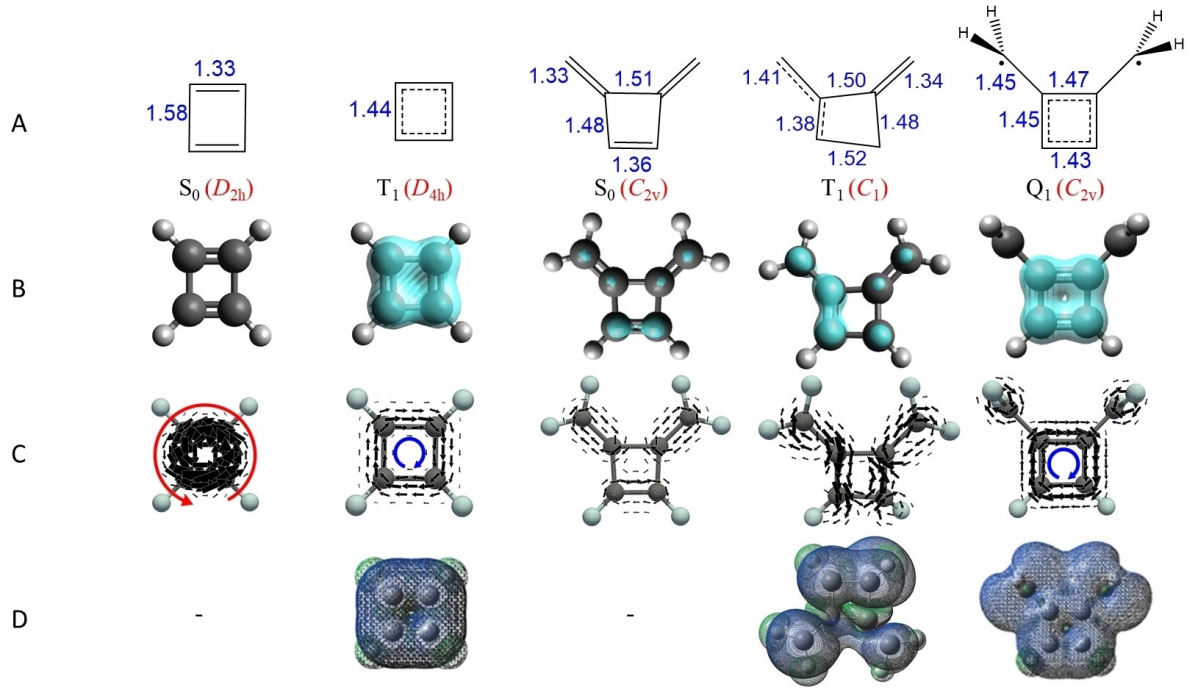

Figure 2. (A) Structural formulas with optimized bond lengths (blue color) in Å and symmetry (in parenthesis), (B) $EDDB_H$ (isovalues at 0.015 e/Å^3, full-scale MICD plots available in the SI, Figure S5), (C) MICD-π plots, (D) plots of the spin densities (isovalues at 0.0004 e/Å^3) of **CBD** in S_0 and T_1 state and **DMCB** in S_0, T_1 and Q_1 (full-scale MICD plots available in the SI, Figure S8 to S31) respectively.

Table 1. Excited state energy (eV), HOMA, HOMER, ISE (in kcal/mol), FLU, MCI, $NICS(1)_{zz}$, and $EDDB_H(\pi)$ values and dipole moments (in D) of **CBD** in its S_0 and T_1 states and of **DMCB** in its S_0, T_1, and Q_1 states.

compound	E_{rel}	HOMA	HOMER	ISE	FLU	MCI	$NICS(1)_{zz}$	$EDDB_H(\pi)$	μ (D)
^{1}**CBD**	0.0	−4.09	–	36.1	0.104	0.0095	55.6	0.22 (5.5%)	0.0
^{3}**CBD**	0.26	0.31	0.99	−16.3	0.012	0.1257	−17.0	3.16 (79%)	0.0
^{1}**DMCB**	0.0	−1.20	–	−1.6	0.059	0.0272	2.8	1.02 (17%)	0.68
^{3}**DMCB**[a]	2.52	−1.36	−1.44	−3.2	0.054	0.0192	8.4	1.19 (20%)	0.55
^{3}**DMCB**[b]	1.77	−1.36	−1.42	−2.9	0.070	0.0044	–	1.23 (21%)	0.66
^{1}**DMCB**[c]	3.96	−0.46	−0.57	–	0.049	0.0020	–	2.31 (39%)	2.02
^{5}**DMCB**	4.79	−0.002	0.70	−14.5	0.021	0.1116	−15.6	2.69 (67%)[d]	0.25

[a] Calculations performed at the UB3LYP/6-311G(d,p)//CASSCF(6,6)/ANO-RCC-VTZP level. [b] Calculations performed at the TD-B3LYP/6-311G(d,p)//CASSCF(6,6)/ANO-RCC-VTZP level [c] Calculations performed at the TD-B3LYP/6-311G(d,p) level. [d] Four electrons were considered in the $EDDB_H(\pi)$ analysis, corresponding to those in the CBD ring.

harmonic oscillator model of aromaticity (HOMA) index of **DMCB** in S_0 is negative (antiaromatic), it is much less so than for S_0 **CBD** (Table 1). As for the energy aspects of aromaticity assessed by the isomerization stabilization energy (ISE) approach, **DMCB** has a near-zero value (nonaromaticity), again in contrast to the markedly positive (antiaromatic) value of **CBD** (Table 1 and Scheme S1). The two calculated electronic indices, the fluctuation index (FLU) and the multicenter index (MCI), indicate a weaker antiaromatic character of **DMCB** in S_0 than of **CBD** (Table 1), while both **CBD** and **DMCB** lack electron delocalization according to electron delocalization of delocalized bonds approach ($EDDB_H$, only heavy atoms considered) (Figure 2B). The nonaromatic character of **DMCB** in S_0 is further corroborated by a near-zero nucleus independent chemical shift assessed by the zz-tensor component 1.0 Å above the ring plane ($NICS(1)_{zz}$, Table 1), and a magnetically induced current density (MICD) plot which reveals three local circulations at the C=C bonds instead of a paratropic ring current in the 4-MR (Figure 2C).

To further address the (anti)aromatic character of **DMCB** in the S_0 state, we analyze the results obtained by breathing-orbital valence bond (BOVB) theory (Figure 3A). Most of the S_0 wavefunction contributions correspond to non-aromatic structures (**S_0-I**–**S_0-VII**), *i.e.*, with either one or two exocyclic CC double bonds. Interestingly, zwitterionic resonances (**S_0-II**–**S_0-IV**, **S_0-VI** and **S_0-VII**) present a large overall contribution (64%). In contrast, antiaromatic structures, holding two C=C bonds in the 4-MR and either two radicals at the exocyclic C atoms or

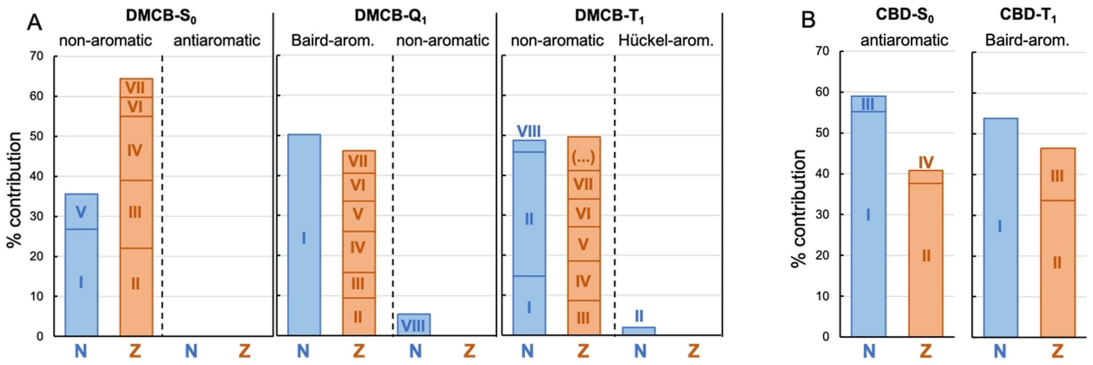

Figure 3. Contribution (Chirgwin-Coulson weights in %) of VB structures (see Figure 1) obtained in the BOVB calculations of (A) **DMCB** in the S_0, Q_1, and T_1 states, and (B) **CBD** in the S_0 and T_1 states. Only one VB structure per set of equivalent structures is displayed, and only structures with contributions $\geq$1 % are included. Individual contributions can be found in Figures S1 and S2. Details on all individual contributions can be found in the SI. N = neutral (blue); Z = zwitterionic (orange).

positive/negative charges (**S_0-VIII** and **S_0-IX**), make minute contributions according to BOVB (each one less than 0.5 % weight). Such S_0 character is radically different from that of **CBD**, where all contributions belong to antiaromatic structures (**S_0-I**–**S_0-IV**), with important participation of zwitterionic structures (**S_0-II** and **S_0-IV**, have a combined weight of 41 %, Figures 3B and S2). Along these lines, the resonance energies (REs) of **DMCB** and **CBD** in S_0, found to be 64.0 and 36.5 kcal/mol (see Tables S4 and S6), respectively, revealed a more pronounced resonance stabilization in the former molecule. The positive RE for **CBD** in S_0 is in agreement with previous computational studies.[77,78] It should be noted that the REs were calculated as the energy difference between two VB wavefunctions, consisting of the dominant VB structure and the full set of VB structures (see Table S3 and S5). However, recently it was shown that large REs are not necessary related to cyclic electron delocalization and aromatic behavior of a given conjugated molecule.[79]

Moreover, $EDDB_H(\pi)$ reveals that for **DMCB** in its S_0 state the π-electrons are weakly delocalized because merely 1.02 (17 %) of the six π-electrons in the π-conjugated network are delocalized (Figure 2B). Therefore, the results gathered from aromaticity descriptors together with the analysis based on VB calculations allow us to univocally identify the **DMCB** S_0 state as non-aromatic. Concretely, the two methylene units prevent the cyclic conjugation that leads to antiaromaticity of the CBD ring, and in addition, they provide a possibility for π-electron donation to or withdrawal from the 4-MR.

The tetraradical state of DMCB: The spin-quintet state (Q_1), *i.e.*, tetraradical (with four unpaired electrons), of **DMCB** shows a C_{2v} symmetric structure, like S_0, but with the planes of the two exocyclic methylene moieties perpendicularly oriented to the plane of the 4-MR (Figure 2A). Furthermore, the BLA of the CC bond lengths of the 4-MR is small and approaching that of **CBD** in its T_1 state (Table 1 and Figure S7). The computed dipole moment of **^{5}DMCB** is modest, revealing a slight charge polarization. The HOMA of **^{5}DMCB** is zero, but the HOMER index, designed especially for assessments of Baird-aromaticity in 4-MR compounds,[65] is clearly approaching that of **CBD** in its T_1 state. Furthermore, the ISE value reveals that **^{5}DMCB** is nearly as aromatic as **^{3}CBD** (−14.5 *vs.* −16.3 kcal/mol, see Scheme S1), and according to the electronic indices, **^{5}DMCB** has an aromatic character close to that of **^{3}CBD**. These findings are further corroborated by the $NICS(1)_{zz}$ value and the MICD plot, which both reveal a diatropic ring current in the 4-MR (Figure 2C). Finally, the spin density reveals π-electron delocalization (Figure 2D), and as noted above, the EDDB value of the 4-MR of **^{5}DMCB** approaches that of **^{3}CBD** (67 % and 79 %, respectively).

One can draw eight (non-equivalent) VB structures with quintet multiplicity (**Q_1-I** to **Q_1-VIII**, Figure 1C) that potentially contribute to the Q_1 state **DMCB**. According to the VB calculations (Figure 3A), the nature of the Q_1 state in **^{5}DMCB** strongly resembles that of **^{3}CBD**. Thus, the most important contribution (49 %) comes from **Q_1-I**, a structure similar to the main component of **^{3}CBD** (Figure 1C, **T_1-I**) which can be labelled as Baird-aromatic. The remaining contributions come from zwitterionic structures which also have four π-electrons in the 4-MR, and which can be tentatively classified as Baird-aromatic as they resemble resonance structures of **^{3}CBD** (Figure 1C, **T_1-II**–**T_1-VII**). In addition, computed REs for **^{5}DMCB** and **^{3}CBD** were found to be very similar (87.0 and 83.3 kcal/mol, respectively, see Table S4 and S6).

The π-electrons of **DMCB** in the Q_1 state are strongly delocalized within the 4-MR with an $EDDB_H(\pi)$ value of 2.69, corresponding to 67 % of four π-electrons (Table 1). Here it is noteworthy that the two p_π electrons at the exocyclic CH_2 moieties are not involved in the conjugated network as these moieties are oriented orthogonally to the plane of the 4-MR. Consequently, the delocalization within the 4-MR of **^{5}DMCB** resembles that of the Baird-aromatic **^{3}CBD** with 3.16 e^- (79 %) delocalized, in stark contrast to 0.22 e^- (5.5 %) in the Hückel-antiaromatic **CBD** in its S_0 state.

Therefore, all these results clearly indicate that **^{5}DMCB** has significant Baird-aromatic character. It is also worth noticing that the lowest singlet state at the **^{5}DMCB** structure, computed at 0.15 (0.02) eV above Q_1 at the RAS-2SF (CASSCF) level, has a strong open-shell (tetraradical) character, as quantified by di- and polyradical indices (Table S10). This implies that the DMCB

moiety holds the capability to produce low-spin states featuring an open-shell character, thus showcasing potential applications in optoelectronics.[80] Its electronic structure can be characterized as the interaction of two triplets on, respectively, the 4-MR and the two methylene units, coupled as an overall singlet. The similarities between the electronic structure of the tetraradical singlet and Q_1, *i.e.*, holding a local triplet in the 4-MR, allow us to identify it as a Baird-aromatic singlet. VB indicates an open-shell character of this state, although diradical instead of tetraradical (see Figure S1).

Lowest triplet and excited singlet of DMCB: Due to the multiconfigurational nature of the T_1 state of **DMCB**, we could not fully optimize it at DFT level. For that reason, we computed the T_1 state at the CASSCF(6,6) level (see Figure S3 and Table S1 and the adjoining discussion). In its T_1 state, **DMCB** (^{3}**DMCB**) is not symmetric (C_1), see Figures 2 and S3. The dipole moment of ^{3}**DMCB** is 0.55 D (Table 1), *i.e.*, slightly lower than that in S_0. The HOMA value of ^{3}**DMCB** is more negative than that of **DMCB** in S_0 and about one third that of **CBD** in S_0 (Table 1), suggesting some antiaromatic character. The HOMER value is also markedly negative. In line with this, the ISE value of ^{3}**DMCB** is −3.2 kcal/mol (Table 1), smaller than that of S_0 **CBD** but still indicative of some weak antiaromatic influence. The MCI value of ^{3}**DMCB** is lower than that of **DMCB** in S_0 suggesting more antiaromatic character in the T_1 state, while FLU indicates the same character for both ^{3}**DMCB** and **DMCB** in S_0. The $NICS(1)_{zz}$ value is positive and suggests a weak paramagnetic ring current, but similar to **DMCB** in S_0, it is difficult to observe any ring current in the MICD plot of ^{3}**DMCB** (Figure 2C). Taken together, ^{3}**DMCB** should be viewed as predominantly non-aromatic but with some modest antiaromatic influence. Is there a more qualitative rationalization of this?

The most important VB structures contributing to the T_1 state of **DMCB** are **T_1-I** and **T_1-II** (Figure 1B), with a combined contribution of 45.8%. Thus, the dominant ones contain four π-electrons inside the ring, yet these structures all have exocyclic CC double bonds and should (again) not be labelled as antiaromatic. The structure with diradical characters at the two exocyclic C atoms and with an antiaromatic CBD ring (**T_1-IX**) makes only a 2% contribution, which is much smaller than that of S_0 **CBD** (59%). The RE for ^{3}**DMCB** was found to be 56.5 kcal/mol, indicating more significant resonance stabilization and reduced antiaromatic character in comparison to S_0 **CBD**. Moreover, $EDDB_H(\pi)$ indicates a moderate delocalization of the π-electrons, with 1.19 delocalized π-electrons (20%) in the π-conjugated network. Thus, **DMCB** in T_1, similar as in S_0, should be described as non-aromatic, not as antiaromatic.

Our analysis also revealed that the B3LYP functional, when compared to EOM-CCSD and CASSCF results, is effective in describing the S_1 state (see Figure S3, Tables S1 and S9, and the adjoining discussion). The structure of S_1, which is nonplanar and C_1 symmetric, is distinctly different from the other states. In the S_1 state, **DMCB** exhibits a dipole moment of 2.02 D, significantly higher than that of T_1 (0.55 D). In terms of electronic indices, we found that the FLU (MCI) value for **DMCB** in the S_1 state is slightly smaller (larger) than the value of the T_1

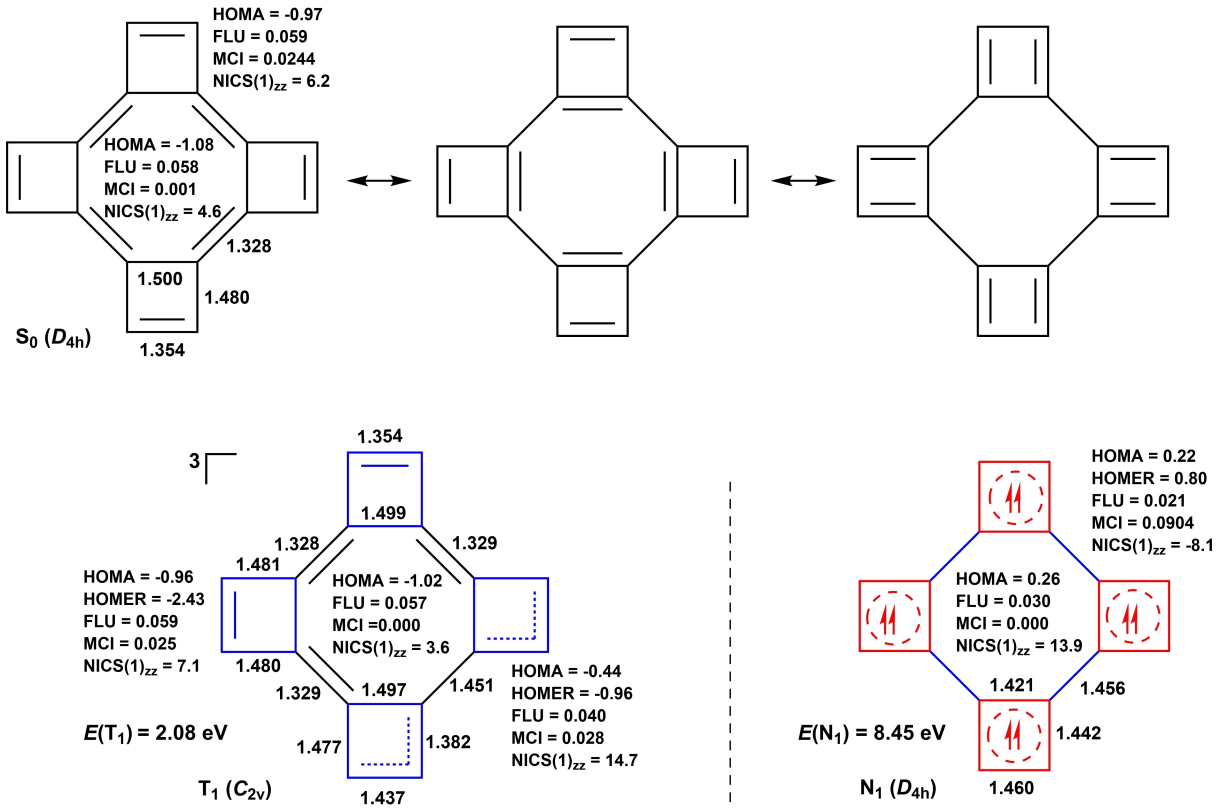

Figure 4. Geometries, relative energies, and aromaticity information on ***c*-4CBD** in its S_0, T_1, and N_1 states calculated at (U)ωB97X-D/6-311G(d,p) level. Energies are given relative to the S_0 state. Bond lengths in Å.

state at TD-DFT level, see Table 1. Still, the MCI value of the S_1 state (0.002) indicates that this state is non-aromatic when compared to the MCI value of the Baird-aromatic ^{3}**CBD** (0.1257, Table 1). Additionally, EDDB calculations revealed that delocalization is present in both states, and our TD-DFT calculations revealed that both the S_1 and T_1 states are mainly described by the HOMO-to-LUMO transition.

DMCB-based macrocycles: Based on the findings of the excited state (anti)aromatic character of **DMCB**, we tested if larger molecules with low-lying high-spin states can be designed, especially utilizing that the Q_1 state of **DMCB** has a Baird-aromatic 4-MR with triplet multiplicity and two localized radicals at the perpendicularly twisted methylene moieties. For this purpose, we explored macrocyclic compounds in which the **DMCB** moieties are linked so that the compounds have nonet states (N_1), *i.e.*, states with eight unpaired electrons, which potentially can be described by four separate 4-MRs that are Baird-aromatic. The first of these, the cyclic oligomer of four 1,2-linked 4-MR (***c*-4CBD**, Figure 4) can be drawn with a second resonance structure depicted as four **DMCB** moieties sharing exocyclic C=C bonds. The second macrocycle (***c*-4BEN4CBD**, Figure 5) is larger and in its S_0 state it can be described as a macrocycle composed of alternating **DMCB** and *para*-xylylene units sharing exocyclic C=C bonds (structure **I**), or alternatively as a cyclic tetramer of phenyl-CBD (structures **II** and **III**). Finally, an even larger macrocycle with acetylene tethers linking the various monocycles of ***c*-4BEN4CBD**, labelled ***c*-4BEN4CBD8C2** (Figure 5), is analyzed in its S_0 and N_1 states. This increases the distance between the 6-MRs and the 4-MRs. Does this enhance the Baird-aromatic character of the 4-MRs in the N_1 state, and does it lead to a lowering of $E(N_1)$? In the two largest macrocycles in their S_0 states there will be a tug-of-war between the antiaromaticity relief of the four 4-MRs leading to a preference of structure **I** of ***c*-4BEN4CBD** (Figure 5) versus aromaticity gain of the four 6-MRs through structures **II** and **III** of ***c*-4BEN4CBD**.

As we deal with larger π-conjugated systems, we apply the range-separated ωB97X-D functional as it provides a better description of the geometries, especially for the T_1 state (see discussion in the ESI, and Figures S35 and S37). The ***c*-4CBD** and ***c*-4BEN4CBD** macrocycles have low-lying T_1 states at energies 2.08 and 0.38 eV (Figures S86 and S87), while the optimized N_1 states of the two species are calculated at, respectively, 8.45 and 2.40 eV above S_0 (Figure S86, and Table S12 for results at other levels of calculation). The remarkable difference in the $E(N_1)$ between ***c*-4CBD** and ***c*-4BEN4CBD** suggests that the 6-MRs largely modify the coupling between the (spin-triplet) 4-MRs. In this regard, it is noteworthy that the $E(N_1)$ of ***c*-4BEN4CBD** is only 1.36 eV higher than that of four isolated **CBD** molecules in their T_1 states with $E(T_1) = 0.26$ eV. Indeed, for ***c***-

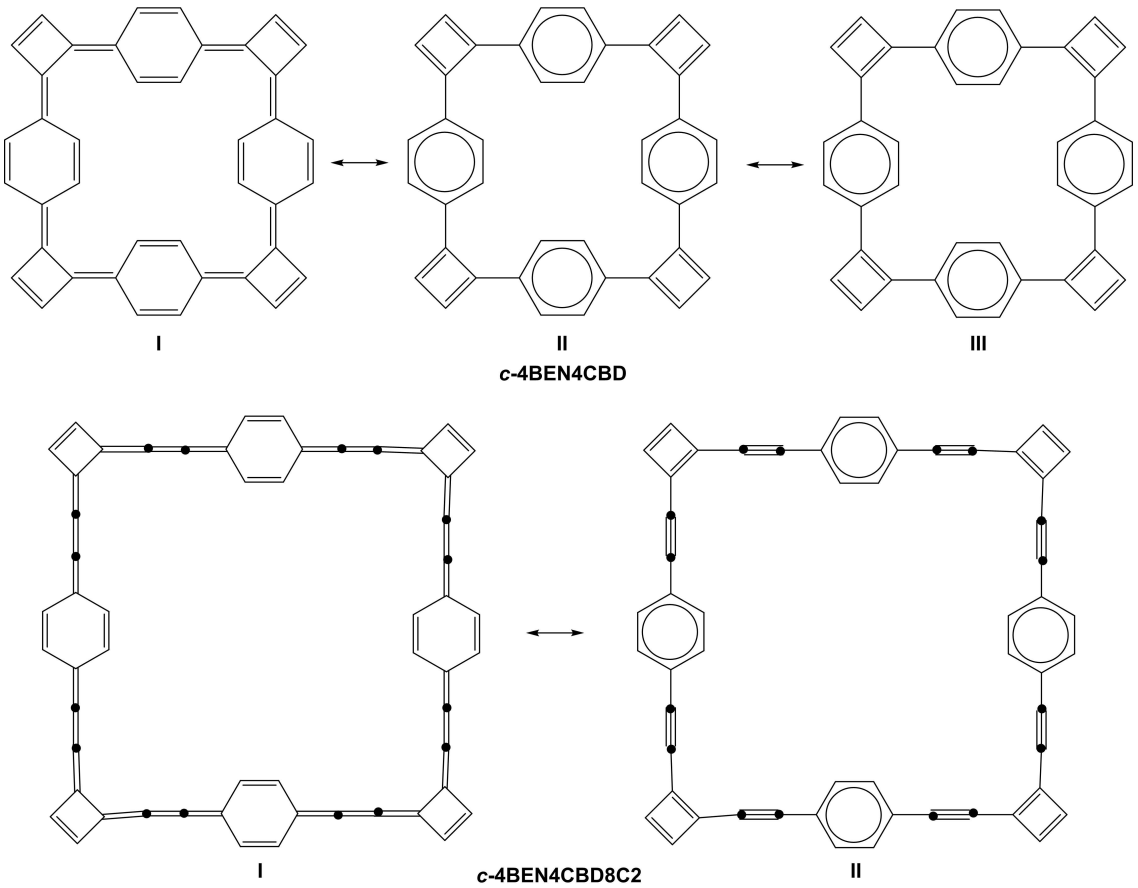

Figure 5. The ***c*-4BEN4CBD** and ***c*-4BEN4CBD8C2** macrocycles with the quinoid/DMCB-type and benzenoid/CBD-type resonance structures shown for ***c*-4BEN4CBD**. A more comprehensive set of resonance structures is shown in Figure S90.

4BEN4CBD8C2, with even more distantly separated 4-MRs, the optimized N_1 state is found at an energy 0.37 eV relative to S_0 (*vide infra*), indicating that a truly high-spin state will be thermally populated in this molecule. Remarkably, this $E(N_1)$ energy is even lower than that of four isolated **CBD** molecules, each in their T_1 states, by 0.67 eV.

To get an understanding of these species, we first analyzed ***c*-4CBD** and its potential antiaromaticity in the S_0 state. For the 4-MRs, the CC bond lengths do not resemble those of S_0 **CBD**, and despite that the HOMA value is markedly negative (Figure 4), it is less so than in S_0 **CBD** (Table 1). Furthermore, the MICD plot indicates some weak paratropic ring currents in the 4-MRs but the current density is mostly described by local circulations at the C=C bonds linking the four 4-MRs (Figure 6A). The latter is in line with the $NICS(1)_{zz}$ values (Figure 4), which are only moderately positive when compared to that of **CBD** in S_0 (55.4, Table 1). Also the FLU and MCI values indicate less antiaromatic character of the 4-MRs of ***c*-4CBD** than in S_0 **CBD** (Figure 4 and Table 1). Thus, ***c*-4CBD** in S_0 has some modest antiaromatic character, but not to the extent that this feature alone should lead to a low chemical persistence.

Going to the T_1 state, the symmetry of the molecule is reduced to C_{2v} with three inter-ring CC bond lengths of 1.33 Å and one of 1.45 Å (see Figure 4). The electronic FLU and MCI as well as the geometric HOMA indicate even less antiaromatic character than in the S_0 state of ***c*-4CBD**, and with EDDB the extent of the delocalized electrons increases significantly from 5.60 e in S_0 to 10.71 e in T_1 (Figure 6B, for a difference between functionals, see Table S11), yet the delocalization is unsymmetric and this is also revealed by the spin density (Figure 6C).

Now, for the N_1 state of ***c*-4CBD**, the electronic and geometric indices suggest a rather strong Baird-aromatic character as the FLU, MCI and HOMER values are similar to those of **CBD** in its Baird-aromatic T_1 state. The spin density also reveals a uniform distribution of the α-spin excess (Figure 6C). One can further note that the inter-ring CC bond lengths (1.456 Å, Figure 4) are longer by ~0.13 Å than those in the S_0 and T_1 states, indicative of lower π-bond order of these bonds in the N_1 state. Within the 4-MRs the CC bond lengths only vary by 0.039 Å, and their mean value is similar to that of ^{3}**CBD** (1.441 *vs.* 1.440 Å, respectively). Furthermore, the MICD plot of ^{9}***c*-4CBD** supports a weak Baird-aromaticity of the 4-MRs, in line with the negative $NICS(1)_{zz}$ values of these rings (−8.1). Interestingly, in the central 8-MR the MICD plot reveals a rather strong paratropic ring current (Figure 6A), supported by a moderately positive $NICS(1)_{zz}$ value.

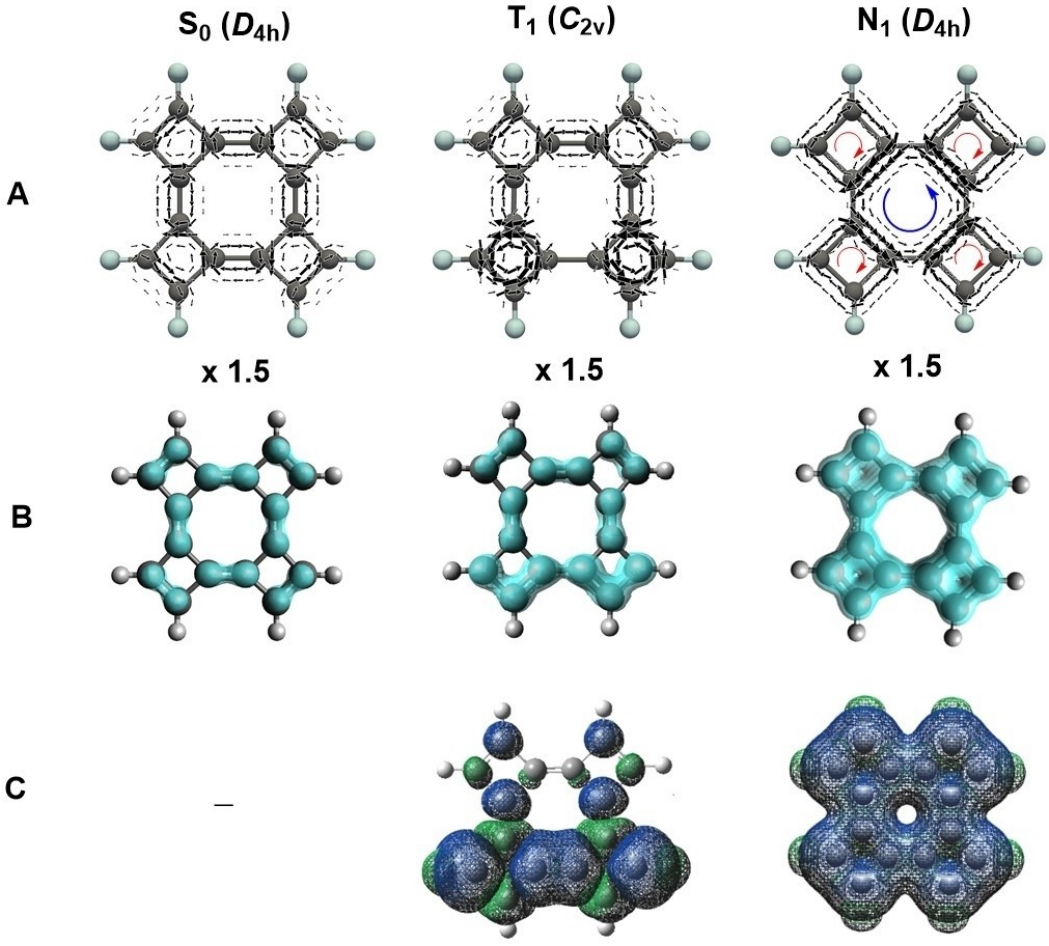

Figure 6. (A) MICD-π, (B) $EDDB_H$, and (C) spin density plot of ***c*-4CBD** in S_0, T_1 and N_1 state computed at the ωB97X-D/6-311G(d,p) level. Full scale MICD plots with high resolution are found in the ESI.

Going to the next larger macrocycle, ***c*-4BEN4CBD**, its HOMA in S_0 is close to zero for the 6-MRs revealing a nonaromatic character (Figure 7) while the value for the 4-MRs is similarly negative as for ***c*-4CBD** suggesting a weak antiaromatic character. Yet, the inter-ring CC bond lengths in S_0 reveal significant *para*-quinoidal character as these bonds are merely 1.352 Å. The NICS(1)$_{zz}$ values are −1.2 for the 6-MRs and 8.5 for the 4-MRs, suggesting nonaromatic character which is confirmed by the MICD plot as neither diatropic nor paratropic ring currents can be identified (Figure 8A). This is corroborated by high FLU and low MCI values. Due to the strong *para*-quinoid character in S_0, the molecule will likely show a tendency to oligomerize unless bulky and kinetically stabilizing substituents are attached.

With regard to the tentative synthesis, one may argue that the 4-MRs can be formed from properly substituted tetrahedranes which photochemically can rearrange to the correspondingly substituted 4-MRs (Figure 9A),[44] building on earlier findings on photochemical formation of substituted **CBD**s. When computing a smaller fragment with trimethylsilyl (TMS) substituents at the two outer C atoms of the CBD ring (Figure 9B), we find that the **CBD** derivative is nearly 20 kcal/mol lower in energy than the tetrahedrane isomer. When substituted with even larger *tert*-butyldimethylsilyl (TBDMS) groups the energy difference between the two isomers is 19.0 kcal/mol (see Figure S91). Clearly, there should be no thermal back-rearrangement to the tetrahedranes for our three macrocycles if the CBD rings are formed in photochemical steps.

In the T_1 state, ***c*-4BEN4CBD** reduces its symmetry from S_4 to C_s with an unequal electron delocalization along the four sides of the molecule as is clear from the EDDB as well as the spin density plot (Figure 8B–C). There are three types of non-equivalent 6-MRs and two types of 4-MRs in the molecule, and the 6-MRs range from aromatic to nonaromatic while the 4-MRs are nonaromatic or slightly antiaromatic depending on the aromaticity index considered. The HOMA values for the 4-MRs suggest that these rings are just slightly antiaromatic, as they

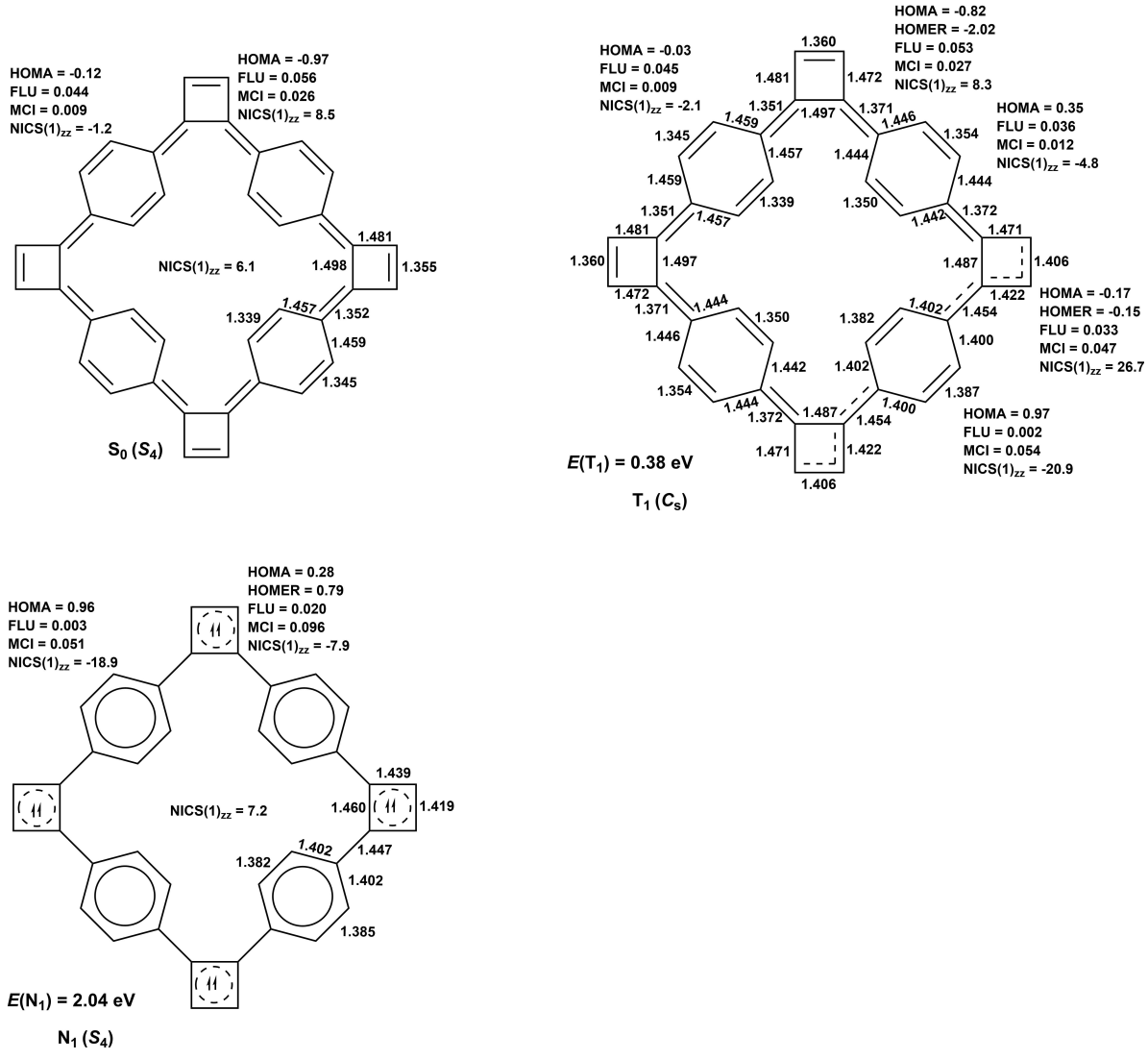

Figure 7. Geometries, relative energies, and aromaticity information for ***c*-4BEN4CBD** in its S_0, T_1, and N_1 states computed at the (U)ωB97X-D/6-311G(d,p) level. Energies are given relative to the S_0 state. Bond lengths in Å.

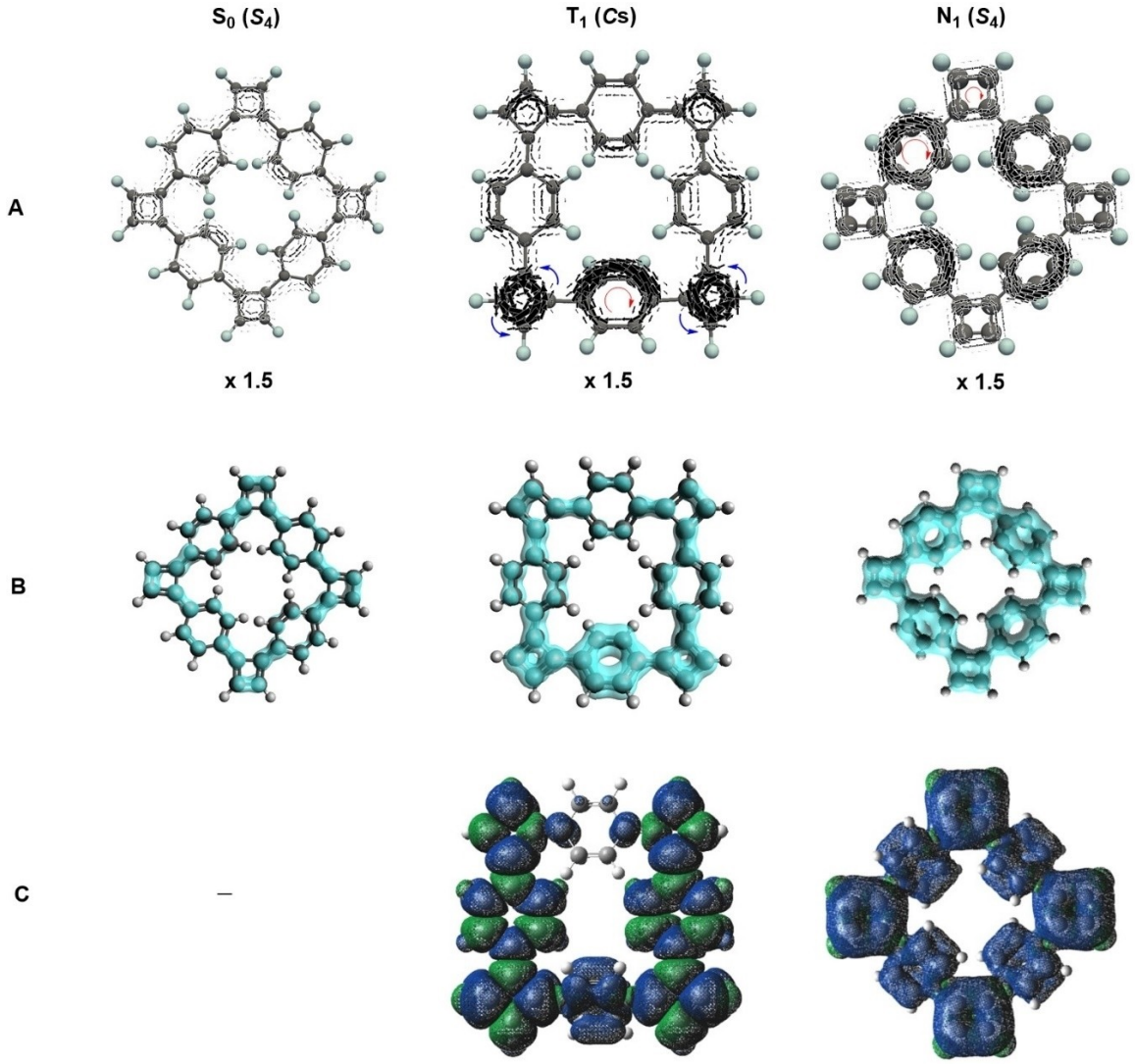

Figure 8. (A) MICD-π, (B) $EDDB_H$, and (C) spin density plot of ***c*-4BEN4CBD** in S_0, T_1, and N_1 state computed at the ωB97X-D/6-311G(d,p) level. Full scale MICD plots with high resolution are found in the ESI.

are much less negative than for **CBD** in S_0 (−0.82 and −0.17 *versus* −4.09, Figure 7 and Table 1). The values of the HOMER index, developed to identify Baird-aromatic 4-MRs,[65] suggest that the 4-MRs are far from Baird-aromatic. These results are supported by the $NICS(1)_{zz}$ values (Figure 7), which are positive, yet significantly less than for S_0 **CBD**. The relatively high (low) FLU (MCI) values further corroborate the results from the magnetic and geometric descriptors (Figure 7).

As per our hypothesis, the N_1 state of the ***c*-4BEN4CBD** has a better ability than ***c*-4CBD** to accommodate four Baird-aromatic 4-MRs (*cf.*, four separate ^{3}**CBD**s) connected to (or separated by) four Hückel-aromatic 6-MRs (*cf.*, benzene rings). With regard to the energy of the N_1 state, it is placed in a range accessible from the singlet (triplet) manifolds, as the N_1 state is placed less than 0.6 eV above S_1 and T_1 (2.40, 2.03, and 0.38 eV, respectively, see Figure S87). Moreover, electronic structure calculations at the RAS-4SF/6-31G(d) level indicate that the four 4-MRs are antiferromagnetically coupled, with a singlet-nonet vertical energy gap of 0.85 eV.

Compared to the S_0 state, both ring types exhibit small bond length alternations in ^{9}***c*-4BEN4CBD** (Figure 7). The 6-MRs are Hückel-aromatic according to HOMA and the 4-MRs have positive HOMER values only slightly lower than that of T_1 **CBD**, suggesting that they are Baird-aromatic. The low (high) FLU (MCI) values also suggest that the 6- and 4-MRs are, respectively, Hückel- and Baird-aromatic (Figure 7). The $NICS(1)_{zz}$ values for the 4-MRs and 6-MRs are all negative, although less so for the 4-MR indicative of only a slight aromatic character compared to the 6-MRs. The latter is corroborated by the MICD plot, which reveals weakly diatropic ring-currents in the 4-MRs and stronger such character in the 6-MRs (Figure 8). Thus, in the N_1 state the 4-MRs act as Baird-aromatic **CBD** units while the 6-MRs are Hückel-aromatic benzene moieties.

Having established that ^{9}***c*-4BEN4CBD** is (somewhat) Baird-aromatic in the 4-MRs, the question is if a further lowered N_1

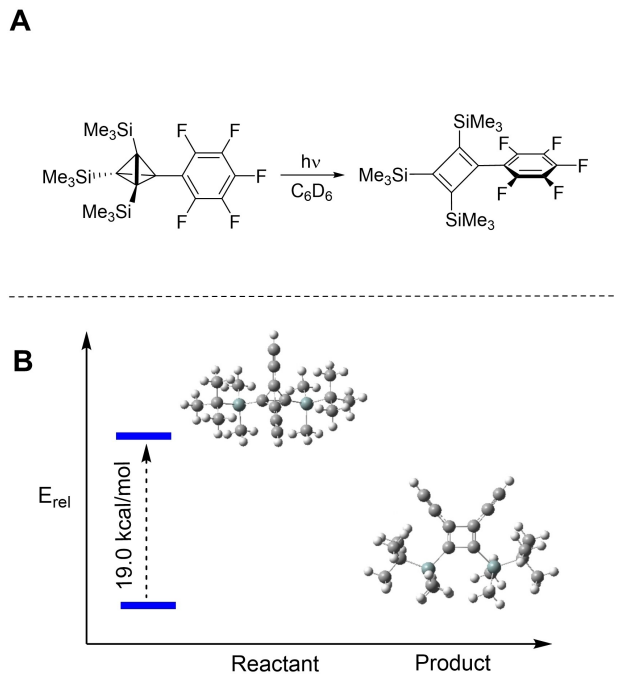

Figure 9. (A) Photoisomerization of perfluoroaryltetrahedrane to perfluoroarylcyclobuta-dienes by Sekiguchi *et al.*,[44] (B) the relative energy (kcal/mol) of the tetrahedrane and the corresponding **CBD** derivative calculated at the B3LYP/6-311G(d,p) level.

state can be achieved by expanding the distance between the 4-MRs. This is addressed with ***c*-4BEN4CBD8C2**, and as noted above, this macrocycle has an $E(N_1)$ of 0.37 eV. This means that by incorporation of spacers between the 4-MRs the $E(N_1)$ is reduced from 8.45 eV for ***c*-4CBD** via 2.40 eV for ***c*-4BEN4CBD** to a value that should correspond to a thermally accessible nonet state.

For ***c*-4BEN4CBD8C2**, we performed conformational searches in both the S_0 and N_1 states of this macrocycle. According to the (U)ωB97X-D calculations the most stable structures are completely planar, yet, in each state there are four higher-energy minima, with one, two, three of four benzene rings oriented perpendicularly to the molecular plane and with relative energies from 3 to 13 kcal/mol above the S_0 or N_1 planar minima (Table S13). The lower-energy of these conformers will be populated at ambient temperatures. Furthermore, the energies of the transition states that lead from the planar to the fully perpendicular structures of ***c*-4BEN4CBD8C2** in the S_0 and N_1 states are 14.0 and 14.9 kcal/mol, respectively (Figure S91 and Figure S92). The optimized geometry of ***c*-4BEN4CBD8C2** in S_0 (Figure 10) reveals 4-MRs with CC bond lengths that resemble those of **CBD** in S_0, opposite to what is found in ***c*-4BEN4CBD** and ***c*-4CBD** where only one CC bond is a short olefinic bond. The HOMA value of ***c*-4BEN4CBD8C2** also indicates a strong antiaromaticity of the 4-MRs approaching that of **CBD** in S_0 (Table 1), and the $NICS(1)_{zz}$, MCI and FLU values (Figure 10) as well as the MICD plot (Figure 11A) agree with that description. One may thus conclude that ***c*-4BEN4CBD8C2** will not be an overly stable molecule unless having sterically congestive substituents that hinder its dimerization (Figure 9). With regard to the 6-MRs, all indices reveal strongly Hückel-aromatic benzene rings.

In the N_1 state, the four 4-MRs of ***c*-4BEN4CBD8C2** are less Baird-aromatic than those of ***c*-4BEN4CBD** according to the geometric HOMER index, yet according to MCI there is only a slight attenuation, and according to $NICS(1)_{zz}$ the aromaticity of the two macrocycles in their N_1 states are essentially the same (Figure 10). One can also note clear diatropic ring currents in the 4-MRs, although much weaker than in the 6-MRs (Figure 11A). The low Baird-aromaticity according to HOMER can be rationalized through the significant variation in CC bond lengths in the 4-MR from 1.345 to 1.481 Å. With regard to the 6-MRs they are equally aromatic in the N_1 state as in the S_0 state according to all indices and should thus be regarded as benzene rings. One can note a slight tendency towards a

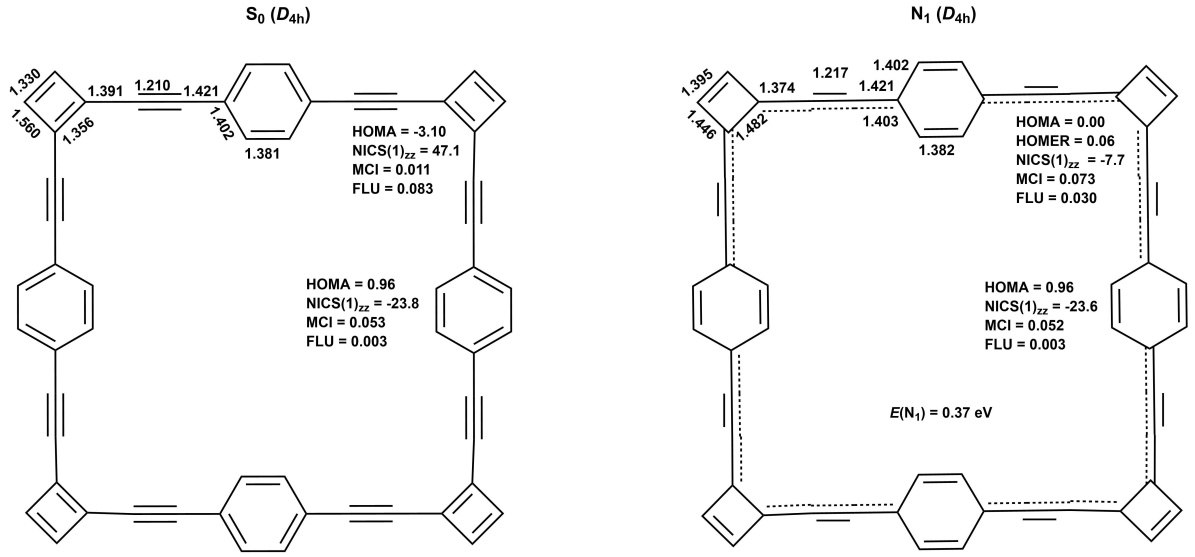

Figure 10. Geometry and aromaticity information for ***c*-4BEN4CBD8C2** in its S_0 and N_1 states computed at the (U)ωB97X-D/6-311G(d,p) level. Bond lengths in Å.

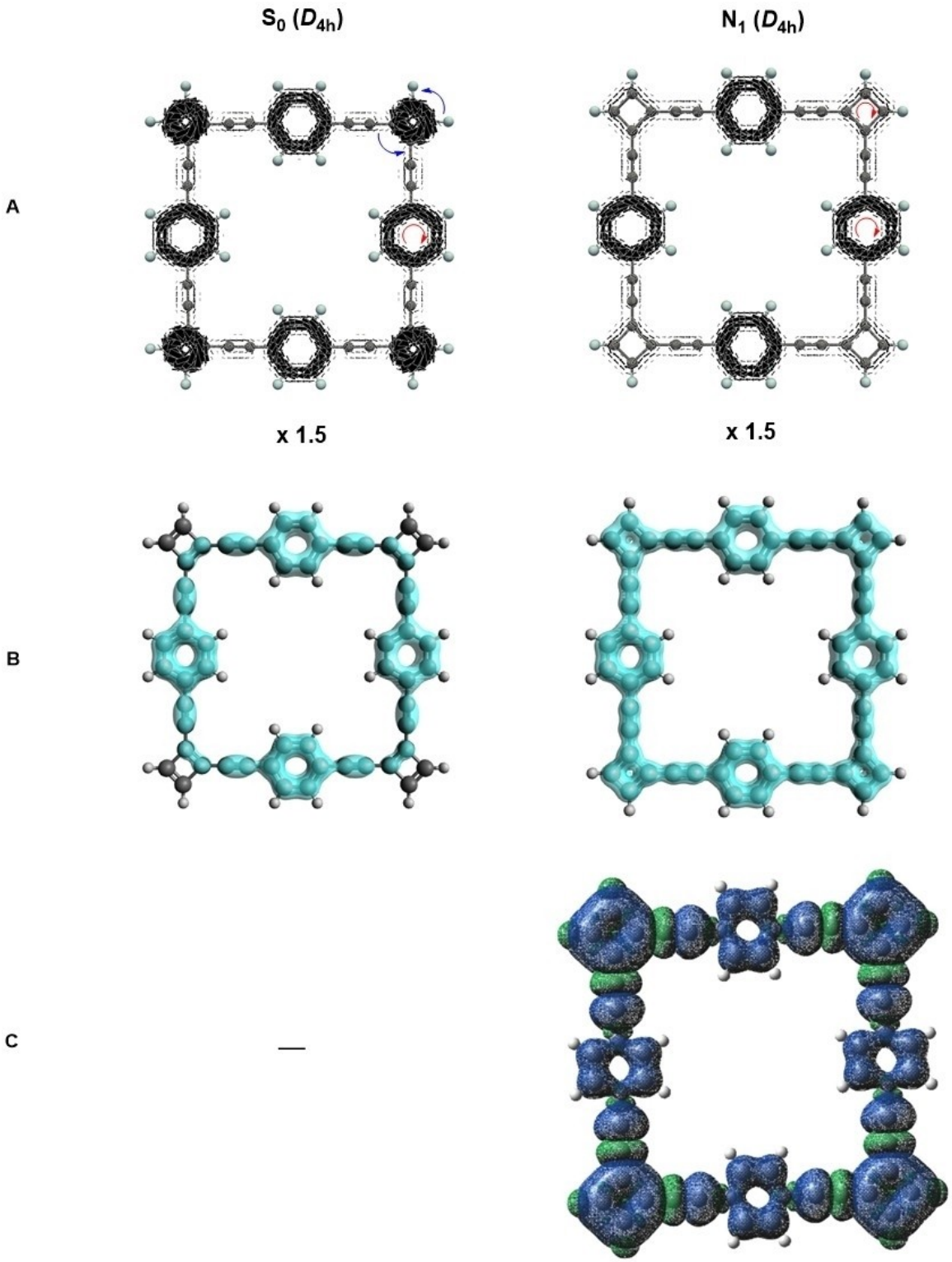

Figure 11. (A) MICD-π, (B) $EDDB_H$, and (C) spin density plots of ***c*-4BEN4CBD** in S_0 and N_1 state, calculated at the ωB97X-D/6-311G(d,p) level. Full scale MICD plots with high resolution are found in the ESI.

quinoidal character, yet the HOMA value is still close to maximal. Finally, the $EDDB_H$ reveal as drastically enhanced delocalization (Figure 11B) and the spin density reveals excess of α-spin density at the 4-MRs (Figure 11C).

At this point, it is relevant to ask why the Baird-aromatic character is (slightly) weaker in ^{9}***c*-4BEN4CBD8C2** than in ^{9}***c*-4BEN4CBD**? Based on the geometries of the two macrocycles in their N_1 states, it is apparent that the 4-MRs interact stronger

with the linkers when using 1,4-diethynylbenzene units than when using *para*-phenylene units, as the exocyclic CC bonds from the 4-MRs are, respectively, 1.447 and 1.374 Å. The direct linking of potentially Baird-aromatic units with potentially Hückel-aromatic units should be desirable as the latter (seeking maximal aromaticity) will provide minimal interaction with the former. As longer linkers one may thus propose biphenyl or naphthyl linkers instead of the 1,4-diethynyl(benzene) linkers in ***c*-4BEN4CBD8C2**. Hence, there are a number of further possibilities for tailoring the macrocycles than those explored herein, and it is ideally done in a combined computational and synthetic effort.

Conclusions

Herein, we have explored a structural motif, the 3,4-dimethylenecyclobutene (**DMCB**), which exhibits properties that are fundamentally interesting as well as potentially useful for organic materials applications. Our focus is on its (anti)aromaticity in the ground and lowest few electronically excited states; the lowest two singlet states (S_0 and S_1), the lowest triplet (T_1) and the lowest quintet state (Q_1), analyzed in terms of Hückel-antiaromaticity and Baird-aromaticity of, respectively, a closed-shell and an open-shell biradical cyclobutadienyl unit. We reveal that the S_0 and T_1 states are nonaromatic while the Q_1 state is Baird-aromatic with a four-membered ring primarily described by a triplet biradical cyclobutadiene (**CBD**) ring. This description is provided by valence bond theory as well as different computed aromaticity descriptors (electronic, geometric, magnetic, and energetic).

Based on the **DMCB** scaffold we designed three macrocycles where the largest according to our computations has a nonet state (N_1) at an energy 0.37 eV above its S_0 state. In their N_1 states these three macrocycles can, to various extents, be described by four Baird-aromatic CBD moieties, in the largest separated by isolating 1,4-diethynylbenzene moieties. To block the potential oligomerization of these macrocycles in the S_0 state via dimerization of the CBD moieties, we explored the effect of substitution by sterically congestive silyl groups.

In summary, through our computational investigation of the fundamental excited state properties of the **DMCB** molecule, we identify a set of macrocycles with presumably useful optoelectronic properties that should be interesting targets for experimental realization.

Supporting Information

The authors have cited additional references within the Supporting Information.[81]

Acknowledgements

We are grateful for a postdoctoral fellowship from the Wenner-Gren Foundations for P.P. (UPD2021-0205) and the Swedish Research Council for financial support of H.O. (grant 2019-05618). D.C. acknowledges support by the Spanish "Ministerio de Ciencia e Innovación" (projects PID2019-109555GB–I00 and PID2022-136231NB–I00), and S.R. acknowledges support by the Serbian Ministry of Science, Technological Development and Innovation (Agreement No.451-03-47/2023-01/200122). J. C. R., F.C., and D. C. are grateful to the Transnational Common Laboratory QuantumChemPhys (Theoretical Chemistry and Physics at the Quantum Scale, grant number ANR-10-IDEX-03-02) established between the Université de Bordeaux (UB), Euskal Herriko Unibertsitatea (UPV/EHU) and DIPC. The authors acknowledge the financial support received from LTCSarea on behalf of the Department of Education and Presidency of the Basque Government. The computations were enabled by resources provided by the National Academic Infrastructure for Supercomputing in Sweden (NAISS) and the Swedish National Infrastructure for Computing (SNIC) at the National Supercomputer Center (NSC), Linköping, Sweden.

Conflict of Interests

The authors declare no conflict of interest.

Data Availability Statement

The data that support the findings of this study are available in the supplementary material of this article.

Keywords: Aromaticity · Baird's rule · Computational molecular design · High-spin molecules · Valence bond theory

[1] A. T. Blomquist, P. M. Maitlis, *Proc. Chem Soc.* **1961**, 332.
[2] W. D. Huntsman, H. J. Wristers, *J. Am. Chem. Soc.* **1963**, *85*, 3308–3309.
[3] L. Skatebd, S. Solomon, *J. Am. Chem. Soc.* **1965**, *87*, 4506–4513.
[4] R. D. Brown, F. R. Burden, *Chem. Commun.* **1966**, *14*, 448–449.
[5] W. D. Huntsman, H. J. Wristers, *J. Am. Chem. Soc.* **1967**, *89*, 342–347.
[6] R. D. Brown, F. R. Burden, A. J. Jones, J. E. Kent, *Chem. Commun.* **1967**, 808–809.
[7] K. L. Allinger, C. Gilardeau, L. W. Chow, *Tetrahedron* **1968**, *24*, 2401–2406.
[8] A. Skancke, *Acta Chem. Scand.* **1968**, *22*, 3239–3244.
[9] B. A. W. Coller, M. L. Heffernan, A. J. Jones, *Aust. J. Chem.* **1968**, *21*, 1807–1826.
[10] D. W. T. Griffith, J. E. Kent, M. F. O'Dwyer, *Aust. J. Chem.* **1972**, *25*, 241–256.
[11] B. A. Hess, L. J. Schaad, *Aust. J. Chem.* **1972**, *25*, 2231–2232.
[12] F. Toda, P. Garratt, *Chem. Rev.* **1992**, *92*, 1685–1707.
[13] D. J. Pasto, D. K. Mitra, *J. Org. Chem.* **1982**, *47*, 1381–1382.
[14] D. J. Pasto, *J. Org. Chem.* **1985**, *50*, 4465–4467.
[15] X. Huang, B. Z. Chen, P. Li, D. W. Ji, J. Liu, H. Zheng, S. N. Yang, Y. C. Hu, B. Wan, X. P. Hu, C. Fu, Y. Huang, J. Zheng, Q. A. Chen, S. Ma, *Nat. Chem.* **2022**, *14*, 1185–1192.
[16] M. H. Van der Veen, M. T. Rispens, H. T. Jonkman, J. C. Hummelen, *Adv. Funct. Mater.* **2004**, *14*, 215–223.
[17] C. Y. Lin, A. Krantz, *J. Chem. Soc. Chem. Commun.* **1972**, 1111–1112.
[18] T. Bally, S. Chai, M. Neuenschwander, Z. Zhu, *J. Am. Chem. Soc.* **1997**, *119*, 1869–1875.
[19] G. Maier, *Angew. Chem. Int. Ed.* **1974**, *13*, 425–438.
[20] H. Hopf, *Angew. Chem. Int. Ed.* **2013**, *52*, 12224–12226.
[21] C. Hong, J. Baltazar, J. D. Tovar, *Eur. J. Org. Chem.* **2022**, *2022*, e202101343.
[22] C. T. Blood, R. P. Linstead, *J. Chem. Soc.* **1952**, 2263–2268.
[23] K. Hafner, K. F. Bangert, V. Orfanos, *Angew. Chem. Int. Ed.* **1967**, *6*, 451–452.

[24] G. Maier, S. Pfriem, U. Schafer, M. Rudolf, *Angew. Chem. Int. Ed.* **1978**, *17*, 520–521.
[25] H. Irngartinger, N. Riegler, D.-C. K.-D. Malsch, D.-C. K.-A. Schneider, G. Maier, *Angew. Chem. Int. Ed.* **1980**, *19*, 211–212.
[26] K. Hafner, H. U. Süss, *Angew. Chem. Int. Ed.* **1973**, *12*, 575–577.
[27] I. Gutman, S. Bosanac, *Tetrahedron* **1977**, *33*, 1809–1812.
[28] A. Moyano, J. C. Paniagua, *J. Org. Chem.* **1986**, *51*, 2257–2266.
[29] A. Moyano, J. C. Paniagua, *J. Org. Chem.* **1991**, *56*, 1858–1866.
[30] J.-P. Malrieu, C. Lepetit, M. Gicquel, J.-L. Heully, P. W. Fowlerc, R. Chauvin, *New J. Chem.* **2007**, *31*, 1918.
[31] J.-i. Aihara, *Phys. Chem. Chem. Phys.* **2016**, *18*, 11847.
[32] S. Zilberg, Y. Haas, *J. Phys. Chem. A* **1998**, *102*, 10851–10859.
[33] H. Ottosson, *Nat. Chem.* **2012**, *4*, 969–971.
[34] M. Rosenberg, C. Dahlstrand, K. Kilså, H. Ottosson, *Chem. Rev.* **2014**, *114*, 5379–5425.
[35] R. Papadakis, H. Ottosson, *Chem. Soc. Rev.* **2015**, *44*, 6472–6493.
[36] J. Yan, T. Slanina, J. Bergman, H. Ottosson, *Chem. Eur. J.* **2023**, *29*, e202203748.
[37] H. Ottosson, K. Kilså, K. Chajara, M. C. Piqueras, R. Crespo, H. Kato, D. Muthas, *Chem. Eur. J.* **2007**, *13*, 6998–7005.
[38] M. Rosenberg, H. Ottosson, K. Kilså, *Phys. Chem. Chem. Phys.* **2011**, *13*, 12912–12919.
[39] S. Yadav, O. El Bakouri, K. Jorner, H. Tong, C. Dahlstrand, M. Solà, H. Ottosson, *Chem. Asian J.* **2019**, *14*, 1870–1878.
[40] K. Jorner, R. Emanuelsson, C. Dahlstrand, H. Tong, A. V. Denisova, H. Ottosson, *Chem. Eur. J.* **2014**, *20*, 9295–9303.
[41] A. Sekiguchi, M. Tanaka, T. Matsuo, H. Watanabe, *Angew. Chem. Int. Ed.* **2001**, *40*, 1675–1677.
[42] A. Sekiguchi, T. Matsuo, M. Tanaka, H. Watanabe, M. Nakamoto, *Russ. Chem. Bull.* **2004**, *53*, 1109–1115.
[43] G. Maier, J. Neudert, O. Wolf, *Angew. Chem. Int. Ed.* **2001**, *40*, 1674–1675.
[44] Y. Inagaki, M. Nakamoto, A. Sekiguchi, *J. Am. Chem. Soc.* **2011**, *133*, 16436–16439.
[45] A. D. Becke, *J. Chem. Phys.* **1993**, *98*, 5648.
[46] P. J. Stephens, F. J. Devlin, M. J. Frisch, C. F. Chabalowski, *J. Phys. Chem.* **1994**, *98*, 11623.
[47] J.-D. Chai, M. Head-Gordon, *Phys. Chem. Chem. Phys.* **2008**, *10*, 6615.
[48] D. Casanova, M. Head-Gordon, *Phys. Chem. Chem. Phys.* **2009**, *11*, 9779–9790.
[49] D. Casanova, *WIREs Comput. Mol. Sci.* **2022**, *12*, e1561.
[50] J. H. van Lenthe, G. G. Balint-Kurti, *Chem. Phys. Lett.* **1980**, *76*, 138–142.
[51] J. H. van Lenthe, G. G. Balint-Kurti, *J. Chem. Phys.* **1983**, *78*, 5699–5713.
[52] J. Verbeek, J. H. van Lenthe, *J. Mol. Struct.* **1991**, *229*, 115–137.
[53] S. Shaik, P. C. Hiberty, *A Chemist's Guide to Valence Bond Theory*, Wiley-Interscience, New York, **2008**.
[54] P. C. Hiberty, J. P. Flament, E. Noizet, *Chem. Phys. Lett.* **1992**, *189*, 259–265.
[55] P. C. Hiberty, S. Humbel, C. P. Byrman, J. H. van Lenthe *J. Chem. Phys.* **1994**, *101*, 5969–5976.
[56] P. C. Hiberty, S. Shaik, *Theor. Chem. Acc.* **2002**, *108*, 255–272.
[57] P. v. R. Schleyer, F. Puhlhofer, *Org. Lett.* **2002**, *4*, 2873–2876.
[58] J. Zhu, K. An, P. v. R. Schleyer, *Org. Lett.* **2013**, *15*, 2442–2445.
[59] E. Matito, M. Duran, M. Solà, *J. Chem. Phys.* **2005**, *122*, 014109.
[60] M. Giambiagi, M. S.de Giambiagi, C. D. dos Santos, A. P. de Figueiredo, *Phys. Chem. Chem. Phys.* **2000**, *2*, 3381–3392.
[61] P. Bultinck, R. Ponec, S. Van Damme, *J. Phys. Org. Chem.* **2005**, *18*, 706–718.
[62] D. W. Szczepanik, M. Andrzejak, K. Dyduch, E. Żak, M. Makowski, G. Mazur, J. Mrozek, *Phys. Chem. Chem. Phys.* **2014**, *16*, 20514–20523.
[63] D. W. Szczepanik, M. Andrzejak, J. Dominikowska, B. Pawełek, T. M. Krygowski, H. Szatylowicz, M. Solà, *Phys. Chem. Chem. Phys.* **2017**, *19*, 28970–28981.
[64] M. Krygowski, H. Szatylowicz, O. A. Stasyuk, J. Dominikowska, M. Palusiak, *Chem. Rev.* **2014**, *114*, 6383–6422.
[65] E. M. Arpa, B. Durbeej, *Phys. Chem. Chem. Phys.* **2023**, *25*, 16763–16771.
[66] P. v. R. Schleyer, C. Maerker, A. Dransfeld, H. Jiao, N. J. R. van Eikema Hommes, *J. Am. Chem. Soc.* **1996**, *118*, 6317–6318.
[67] Z. Chen, C. S. Wannere, C. Corminboeuf, R. Puchta, P. v. R. Schleyer, *Chem. Rev.* **2005**, *105*, 3842–3888.
[68] T. A. Keith, R. F. W. Bader, *J. Chem. Phys.* **1993**, *99*, 3669–3682.
[69] T. A. Keith, R. F. W. Bader, *Chem. Phys. Lett.* **1993**, *210*, 223–231.
[70] S. Coriani, P. Lazzeretti, M. Malagoli, R. Zanasi, *Theor. Chim. Acta.* **1994**, *89*, 181–192.
[71] E. Steiner, P. W. Fowler, *J. Phys. Chem. A* **2001**, *105*, 9553–9562.
[72] D. Geuenich, K. Hess, F. Köhler, R. Herges, *Chem. Rev.* **2005**, *105*, 3758–3772.
[73] M. J. Frisch, G. W. Trucks, H. B. Schlegel, G. E. Scuseria, M. A. Robb, J. R. Cheeseman, G. Scalmani, V. Barone, G. A. Petersson, H. Nakatsuji, X. Li, M. Caricato, A. V. Marenich, J. Bloino, B. G. Janesko, R. Gomperts, B. Mennucci, H. P. Hratchian, J. V. Ortiz, A. F. Izmaylov, J. L. Sonnenberg, D. Williams-Young, F. Ding, F. Lipparini, F. Egidi, J. Goings, B. Peng, A. Petrone, T. Henderson, D. Ranasinghe, V. G. Zakrzewski, J. Gao, N. Rega, G. Zheng, W. Liang, M. Hada, M. Ehara, K. Toyota, R. Fukuda, J. Hasegawa, M. Ishida, T. Nakajima, Y. Honda, O. Kitao, H. Nakai, T. Vreven, K. Throssell, J. A. Montgomery, Jr., J. E. Peralta, F. Ogliaro, M. J. Bearpark, J. J. Heyd, E. N. Brothers, K. N. Kudin, V. N. Staroverov, T. A. Keith, R. Kobayashi, J. Normand, K. Raghavachari, A. P. Rendell, J. C. Burant, S. S. Iyengar, J. Tomasi, M. Cossi, J. M. Millam, M. Klene, C. Adamo, R. Cammi, J. W. Ochterski, R. L. Martin, K. Morokuma, O. Farkas, J. B. Foresman, and D. J. Fox, Gaussian, Inc., Wallingford CT, 2016.
[74] E. Epifanovsky, A. T. B. Gilbert, X. Feng, J. Lee, Y. Mao, N. Mardirossian, P. Pokhilko, A. F. White, M. P. Coons, A. L. Dempwolff, Z. Gan, D. Hait, P. R. Horn, L. D. Jacobson, I. Kaliman, J. Kussmann, A. W. Lange, K. U. Lao, D. S. Levine, J. Liu, S. C. McKenzie, A. F. Morrison, K. D. Nanda, F. Plasser, D. R. Rehn, M. L. Vidal, Z. Q. You, Y. Zhu, B. Alam, B. J. Albrecht, A. Aldossary, E. Alguire, J. H. Andersen, V. Athavale, D. Barton, K. Begam, A. Behn, N. Bellonzi, Y. A. Bernard, E. J. Berquist, H. G. A. Burton, A. Carreras, K. Carter-Fenk, R. Chakraborty, A. D. Chien, K. D. Closser, V. Cofer-Shabica, S. Dasgupta, M. De Wergifosse, J. Deng, M. Diedenhofen, H. Do, S. Ehlert, P. T. Fang, S. Fatehi, Q. Feng, T. Friedhoff, J. Gayvert, Q. Ge, G. Gidofalvi, M. Goldey, J. Gomes, C. E. González-Espinoza, S. Gulania, A. O. Gunina, M. W. D. Hanson-Heine, P. H. P. Harbach, A. Hauser, M. F. Herbst, M. Hernández Vera, M. Hodecker, Z. C. Holden, S. Houck, X. Huang, K. Hui, B. C. Huynh, M. Ivanov, Á. Jász, H. Ji, H. Jiang, B. Kaduk, S. Kähler, K. Khistyaev, J. Kim, G. Kis, P. Klunzinger, Z. Koczor-Benda, J. H. Koh, D. Kosenkov, L. Koulias, T. Kowalczyk, C. M. Krauter, K. Kue, A. Kunitsa, T. Kus, I. Ladjánszki, A. Landau, K. V. Lawler, D. Lefrancois, S. Lehtola, R. R. Li, Y. P. Li, J. Liang, M. Liebenthal, H. H. Lin, Y. S. Lin, F. Liu, K. Y. Liu, M. Loipersberger, A. Luenser, A. Manjanath, P. Manohar, E. Mansoor, S. F. Manzer, S. P. Mao, A. V. Marenich, T. Markovich, S. Mason, S. A. Maurer, P. F. McLaughlin, M. F. S. J. Menger, J. M. Mewes, S. A. Mewes, P. Morgante, J. W. Mullinax, K. J. Oosterbaan, G. Paran, A. C. Paul, S. K. Paul, F. Pavošević, Z. Pei, S. Prager, E. I. Proynov, Á. Rák, E. Ramos-Cordoba, B. Rana, A. E. Rask, A. Rettig, R. M. Richard, F. Rob, E. Rossomme, T. Scheele, M. Scheurer, M. Schneider, N. Sergueev, S. M. Sharada, W. Skomorowski, D. W. Small, C. J. Stein, Y. C. Su, E. J. Sundstrom, Z. Tao, J. Thirman, G. J. Tornai, T. Tsuchimochi, N. M. Tubman, S. P. Veccham, O. Vydrov, J. Wenzel, J. Witte, A. Yamada, K. Yao, S. Yeganeh, S. R. Yost, A. Zech, I. Y. Zhang, X. Zhang, Y. Zhang, D. Zuev, A. Aspuru-Guzik, A. T. Bell, N. A. Besley, K. B. Bravaya, B. R. Brooks, D. Casanova, J. Da Chai, S. Coriani, C. J. Cramer, G. Cserey, A. E. Deprince, R. A. Distasio, A. Dreuw, B. D. Dunietz, T. R. Furlani, W. A. Goddard, S. Hammes-Schiffer, T. Head-Gordon, W. J. Hehre, C. P. Hsu, T. C. Jagau, Y. Jung, A. Klamt, J. Kong, D. S. Lambrecht, W. Liang, N. J. Mayhall, C. W. McCurdy, J. B. Neaton, C. Ochsenfeld, J. A. Parkhill, R. Peverati, V. A. Rassolov, Y. Shao, L. V. Slipchenko, T. Stauch, R. P. Steele, J. E. Subotnik, A. J. W. Thom, A. Tkatchenko, D. G. Truhlar, T. Van Voorhis, T. A. Wesolowski, K. B. Whaley, H. L. Woodcock, P. M. Zimmerman, S. Faraji, P. M. W. Gill, M. Head-Gordon, J. M. Herbert, A. I. Krylov, *J. Chem. Phys.* **2021**, *155*, 1–59.
[75] Z. Chen, F. Ying, X. Chen, J. Song, P. Su, L. Song, Y. Mo, Q. Zhang, W. Wu, *Int. J. Quantum. Chem.* **2015**, *115*, 731–737.
[76] L. Song, Y. Mo, Q. Zhang, W. Wu, *J. Comput. Chem.* **2005**, *26*, 514–521.
[77] A. F. Voter, W. A. Goddard III, *J. Am. Chem. Soc.* **1986**, *108*, 2830.
[78] S. Shaik, A. Shurki, D. Danovich, P. C. Hiberty, *Chem. Rev.* **2001**, *101*, 1501–1539.
[79] S. Jain, D. Danovich, S. Radenković, S. Shaik, *Chem. Eur. J.* **2023**, *29*, e202300992.
[80] O. Ostroverkhova, *Chem. Rev.* **2016**, *116*, 13279–13412.
[81] U. Ayachit, *The ParaView Guide: A Parallel Visualization Application*, Kitware, **2015**.

Manuscript received: October 26, 2023
Accepted manuscript online: March 3, 2024
Version of record online: March 27, 2024